

## Radial velocity measurements from LAMOST medium-resolution spectroscopic observations:

### A pointing towards the *Kepler* field

Nian Liu<sup>1</sup>, Jian-Ning Fu<sup>1,\*\*</sup>, Weikai Zong<sup>1,\*\*</sup>, Jianrong Shi<sup>2,3</sup>, Ali Luo<sup>2,3</sup>, Haotong Zhang<sup>2</sup>, Xiangqun Cui<sup>4</sup>, Yonghui Hou<sup>3,4</sup>, Yang Pan<sup>1</sup>, Xinrui Shan<sup>1</sup>, Jianjun Chen<sup>2</sup>, Zhongrui Bai<sup>2,3</sup>, Jianxing Chen<sup>1</sup>, Bing Du<sup>2</sup>, Wen Hou<sup>2</sup>, Yuchen Liu<sup>1</sup>, Hao Tian<sup>2</sup>, Jiangtao Wang<sup>1</sup>, Jiaxin Wang<sup>1</sup>, Kefei Wu<sup>2</sup>, Yuzhong Wu<sup>2</sup>, Hongliang Yan<sup>2,3</sup> and Fang Zuo<sup>2,3</sup>

<sup>1</sup> Department of Astronomy, Beijing Normal University, Beijing 100875, P. R. China;  
*jnfu@bnu.edu.cn, weikai.zong@bnu.edu.cn*

<sup>2</sup> Key Lab for Optical Astronomy, National Astronomical Observatories, Chinese Academy of Sciences, Beijing 100012, P. R. China

<sup>3</sup> School of Astronomy and Space Science, University of Chinese Academy of Sciences, Beijing, 100049, China

<sup>4</sup> Nanjing Institute of Astronomical Optics & Technology, National Astronomical Observatories, Chinese Academy of Sciences, Nanjing 210042, P. R. China

Received 2018 Month Day; accepted 20XX Month Day

**Abstract** Radial velocity is one of key measurements in understanding the fundamental properties of stars, stellar clusters and the Galaxy. A plate of stars in the *Kepler* field were observed in May of 2018 with the medium-resolution spectrographs of LAMOST, aiming to test the performance of this new system which is the upgraded equipment of LAMOST after the first five-year regular survey. We present our analysis on the radial velocity measurements (*RVs*) derived from these data. The results show that slight and significant systematic errors exist among the *RVs* obtained from the spectra collected by different spectrographs and exposures, respectively. After correcting the systematic errors with different techniques, the precision of *RVs* reaches  $\sim 1.3$ ,  $\sim 1.0$ ,  $\sim 0.5$  and  $\sim 0.3$  km/s at  $S/N_r = 10, 20, 50$ , and  $100$ , respectively. Comparing with the *RVs* of the standard stars of the APOGEE survey, our *RVs* are calibrated with a zero-point shift of  $\sim 7$  km/s. The results indicate that the LAMOST medium-resolution spectroscopic system may provide *RVs* in a reasonable accuracy and precision for the selected targets.

**Key words:** technique: spectroscopy — stars: radial velocity — stars: statistics

## 1 INTRODUCTION

The measurements of radial velocities (*RVs*) of a large number of stars plays an important role in understanding the structure of the Galaxy (e.g., Binney & Merrifield 1998) and the kinematics of globular clusters (e.g., Gunn & Griffin 1979). *RVs* are also valuable for the discovery and determination of orbital parameters of binary systems (e.g., Nidever et al. 2002). In recent years, many large surveys provide *RVs* for large samples of stars with high-precision, such as the Sloan Digital Sky Survey for millions of stars (Alam et al. 2015; Eisenstein et al. 2011; Adelman-McCarthy et al. 2006) and the *Gaia* observations on some seven millions of sources with median *RVs* (Gaia Collaboration et al. 2018).

When combined with photometric observations, *RV* variations can offer more precise constraints on the theoretical frameworks of stellar pulsation models (Marconi et al. 2013) and present an unbiased mass determination of the components of eclipsing binary stars (e.g., Vučković et al. 2007). The *Kepler* space mission monitored about 200 000 stars in the region of the constellations Cygnus and Lyrae for a period of  $\sim 4$  yr continuously (Borucki et al. 2010), providing unprecedented high-quality photometric data for many types of variable stars (Gilliland et al. 2010; Prša et al. 2011; Zong et al. 2016). Consequently, to fully exploit the science as offered from these photometric observations, different groups have been organized to provide ground-based spectra as follow-up programs, for instance, APOKASC (Pinsonneault et al. 2014, 2018) and the LAMOST-*Kepler* (LK) project (De Cat et al. 2015; Zong et al. 2018), providing *RVs* for thousands of stars. Nevertheless, multiple visits of specific targets show particular interests in exoplanets or binary detection from periodic *RV* variations (see, e.g., MARVELS in Ge et al. 2008). The LK-project also provides multiple ( $> 4\times$ ) *RVs* for about 500 stars (Zong et al. 2018).

LAMOST<sup>1</sup> is an ideal instrument for spectroscopic observation surveys, which can monitor more than three thousands targets per exposure (Wang et al. 1996; Xing et al. 1998), vastly reducing time consumption to measure *RVs* for a large number of targets. From the pilot and the first 5-yr regular survey, LAMOST obtained more than nine million low-resolution ( $R \sim 1800$ ) spectra (see, e.g., Luo et al. 2015). Since 2017 September, LAMOST was tested with medium-resolution ( $R \sim 7500$ ) spectrographs with two arms covering the wavelength ranges of 630–680 nm and 495–535 nm, respectively (Zong et al. 2018). The bright moon nights in each lunar month are reserved to perform these test observations.

In this paper, we will address an estimation of the precision of *RVs* derived from the current LAMOST pipelines. It is evaluated through time-series spectroscopic observations pointing towards the *Kepler* field. The structure of this paper is organized as follows. The details of observations and data reduction are described in Section 2. We present the techniques to estimate the precision of *RVs* in Section 3, followed by the the comparison with APOGEE *RVs* in Section 4. We give our discussion in Section 5 and conclude our results in Section 6.

---

<sup>1</sup> The Large Sky Area Multi-Object Fiber Spectroscopic Telescope (also called Gou Shoujing Telescope) which is located at the

Table 1: Detailed contents of the LK07 footprint which had been observed by LAMOST equipped with medium-resolution spectrograph during 2018 May.

Observation date	Begin (UT)	End (UT)	Exposure time	Seeing (arcsec)	Parameter
2018 May 24	18:26:16	19:55:33	900 s $\times$ 5	$\sim$ 3.0	7214
2018 May 28	17:23:20	19:39:33	900 s $\times$ 7	$\sim$ 2.6	10375
2018 May 29	17:36:44	19:38:12	600 s $\times$ 9	$\sim$ 2.3	12329
2018 May 30	17:58:56	19:29:23	900 s $\times$ 5	$\sim$ 2.4	7414
2018 May 31	18:02:13	19:32:49	1200 s $\times$ 4	$\sim$ 2.3	6088
Total			25500 s		43420

Notes: The time between begin and end includes the readout time but not the overhead time.

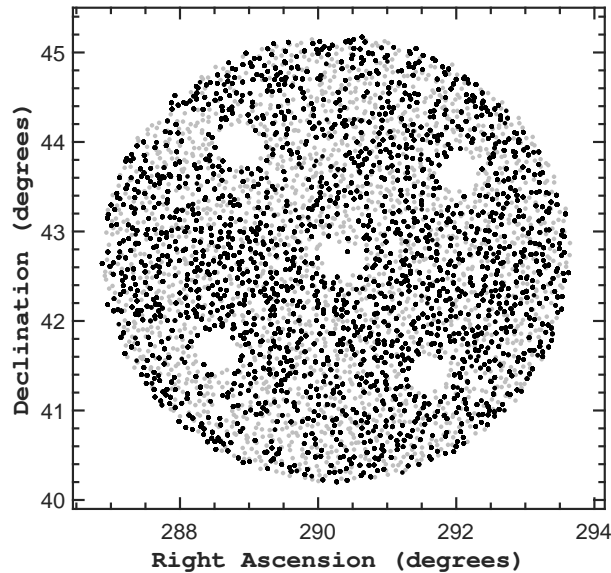


Fig. 1: Sky coverage of all targets (in grey) observed by LAMOST pointing towards the LK07 field. The stars atmospheric parameters derived from LASP are marked in dark.

## 2 OBSERVATIONS AND DATA REDUCTION

### 2.1 Observations

LAMOST has a focal plane of 5 degrees in diameter, equipped with 4000 fibers, hence the telescope can observe 4000 targets (including sky light) per exposure. One circular field in *Kepler* field, LK07, had been chosen to be observed, with an aim to test the precision of *RVs* from the medium-resolution spectra. More details of the classification of each *Kepler* field can be found in De Cat et al. (2015). The central position of LK07 is defined by the coordinates of the bright star HIP 95119 with  $V = 7.03$ ,  $\alpha(2000) = 19 : 31 : 02.82$ , and  $\delta(2000) = +42 : 41 : 13.06$ . This star is used for calculation of wavefronts to reshape the mirrors into good condition. The input targets are chosen based on several criteria as follows, with priority decreasing: two pulsating stars showing particular interests, 6 standard stars, 164 eclipsing binary stars, the rest stars with a similar strategy as in Zong et al. (2018). Figure 1 shows the spatial distribution of 3626 targets which

Table 1 lists the details of the observations of that plate. The footprint had been observed by LAMOST from 2018 May 24, 28 to 31, on five individual nights. This field is given a very high priority to be observed since the *Kepler* field can only be reached during the summer season (see details in De Cat et al. 2015; Zong et al. 2018). Observations can almost start when the LK07 field enters the view of LAMOST, which is confined within two hours before and after the meridian of the central star. The overhead time to prepare for exposure is typically 30 minutes, depending somewhat on the telescope performance and weather conditions. The readout time is about 4 minutes for each exposure. When the exposure is ready, the footprint will be observed continuously until it leaves the view of LAMOST or the twilight is too bright to continue the observation. The latter one is the main reason for stopping the observations in late May. During the observations, the weather condition is typically with a seeing of around 2.5 arcsecs. A total of 30 plates have been obtained with exposures of  $900\text{ s} \times 5$ ,  $900\text{ s} \times 7$ ,  $600\text{ s} \times 9$ ,  $900\text{ s} \times 5$  and  $1200\text{ s} \times 4$ . The total exposure time corresponds to 7.08 hours.

## 2.2 Data reduction

The raw products of LAMOST observations are the two dimensional (2D) CCD frames. For each exposure, a total of 32 (16 blue and 16 red) 2D frames are obtained, with each frame containing 250 raw spectra almost equally spread on the CCD. The first procedure to reduce those raw data is to evaluate the quality of observations and the telescope performance, such as seeing, cloud coverage and checking of polluted light. The 2D frames with good quality are used to produce 1D calibrated spectra by the LAMOST 2D pipeline, which is implemented with procedures similar to those of SDSS (Stoughton et al. 2002). The main tasks of the LAMOST 2D pipeline include dark and bias subtraction, flat field correction, spectral extraction, sky subtraction, and wavelength calibration (see more details in Luo et al. 2015). One notes that the 2D pipeline conducted on the medium-resolution does not contain stacking of sub-exposures and combining of different wavelength bands with these procedures were used for the low-resolution spectra.

The scientific quality of the obtained 1D spectra is evaluated before the atmospheric parameters are calculated. We use the signal-to-noise in *SDSS*-like *r* band (hereafter  $S/N$  for simplification) as the indicator. The spectra with  $S/N$  higher than 10 will be fed to the 1D pipeline to derive the *LASP* parameters and to classify the spectral type. The *RVs* for stars and redshifts for galaxies (or quasi-stellar objects) are also provided through this pipeline. The current version v2.9.7 pipeline is used for the medium-resolution spectra obtained from the LK07 plates. More details of these pipelines can be found in Luo et al. (2012) and Luo et al. (2015).

## 3 ANALYSIS OF RADIAL VELOCITIES

### 3.1 Distributions of *RVs* measurements

The calibrated spectra with high quality can definitely produce atmospheric parameters. However, we will merely discuss the results of the measurement of the precision of *RVs* in this paper. The total number of *RV* measurements obtained from the 30 plates is 43420. The last column of Table 1 lists the individual number



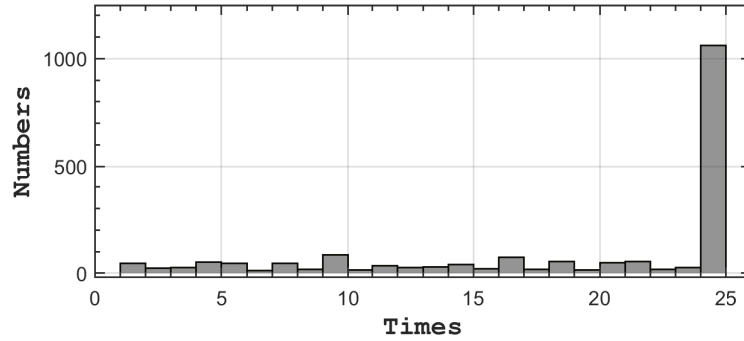


Fig. 2: Distribution of the times for stars derived with RVs from the 25 exposures.

arc<sup>2</sup> was used to calibrate the wavelength for the spectra of the first 5 exposures, while, a Thorium-Argon arc was used for the rest observations. We therefore will not consider the data set from the first 5 exposures in the further analysis. Besides, we checked that the discard of these data do not affect the main scientific results significantly. The total number of stars with RVs is 1880 from the spectra obtained through 2018 May 28-31. Figure 2 shows the distribution of the number of RV determinations that was derived for each of these stars from these 25 exposures. We find that more than half of the targets have 25 RV measurements. The RVs of the same stars visited multiple times can be an excellent practice to examine the robustness of RVs derived from one system (or telescope). We calculate the relative RVs ( $\Delta RV$ s) for each targets by subtracting the weighted mean of their values, where the square of  $S/N$  was used as weight. Figure 3 shows the scatter of the measured  $\Delta RV$ s. From the distribution we can be directly seen that the precision is roughly 1 km/s. However, the outlier measurements are possibly the results from RV variables in particular at high  $S/N$ .

### 3.2 Selection of constant RV stars

To precisely check where the outlier points come from, or concretely to estimate the precision, we need to select the “constant” RV stars first. Stars will fall into our sample if they have relative small  $\Delta RV$  from different plates. The concrete value is taken as 1 km/s since it is the rough precision as estimated from Figure 3. In addition, we find that more than half of 1880 stars whose RVs show standard deviation less than 1 km/s. This criterion can be more strict but the action will lose number of stars to compare the systematic errors in the following sections. The final sample contains 803 stars with 20075 RVs, which are measured from all the 25 plates, called “common constant” stars below.

### 3.3 Analysis of systematic errors

Figure 4 shows the distribution of  $\Delta RV$  where the common constant stars are divided into 16 groups as labeled by their spectrograph IDs. The results suggest very small systematic errors between different spectrographs, as revealed by the weighted values<sup>3</sup> of the  $\Delta RV$ . The values are all near zero but with different standard deviation (see the errorbars in this figure). We note that the symbol itself shows a size of about 200 m/s. The existence of systematic errors between different plates is illustrated in Figure 5. The measured

<sup>2</sup> The Scandium will not be used any longer as a result of comparison to the Thorium-Argon arc.

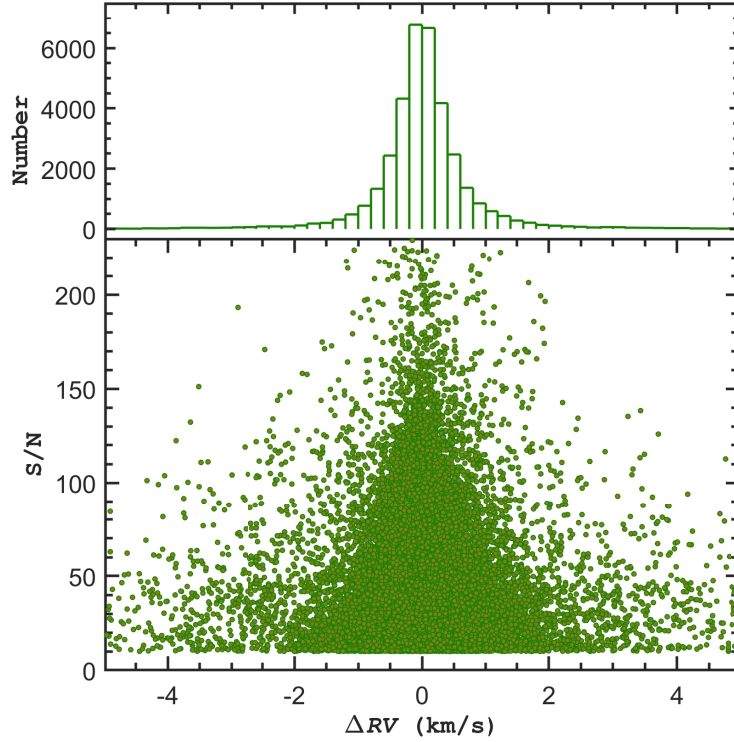


Fig. 3: Distribution of the relative RVs ( $\Delta RV$ ) as a function of the spectra quality  $S/N$  (*bottom panel*). The projection of the  $\Delta RV$  histogram with a bin width of 0.2 km/s is shown in the *top panel*. We note that the long side wings are not shown in this plot.

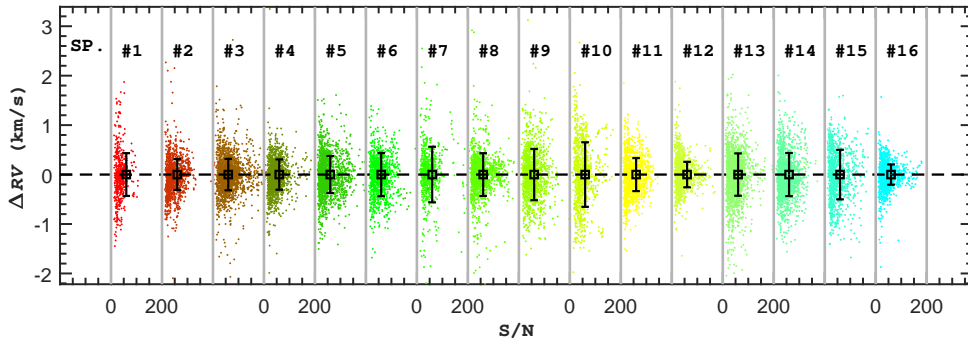


Fig. 4: Distribution of the relative RVs ( $\Delta RV$ ) of the “common constant” stars as a function  $S/N$  (the IDs of spectrographs are marked in numbers on the upper of each panel). The  $S/N$  scale between two consecutive vertical lines is set to be 200. The horizontal dashed line represents the RV under ideal measurement, that is zero, without any deviation. The weight values of each groups are given by open squares with their associated errors (standard deviations). More details are given in the text.

$RV$ s were now divided into 25 groups labeled by the sequence number of the observed plate. We clearly see that there are several  $\Delta RV$  leaps between different nights (as indicated by red vertical lines), typically with values on the order of a few hundreds m/s. In addition, within the same night, shifts are seen between

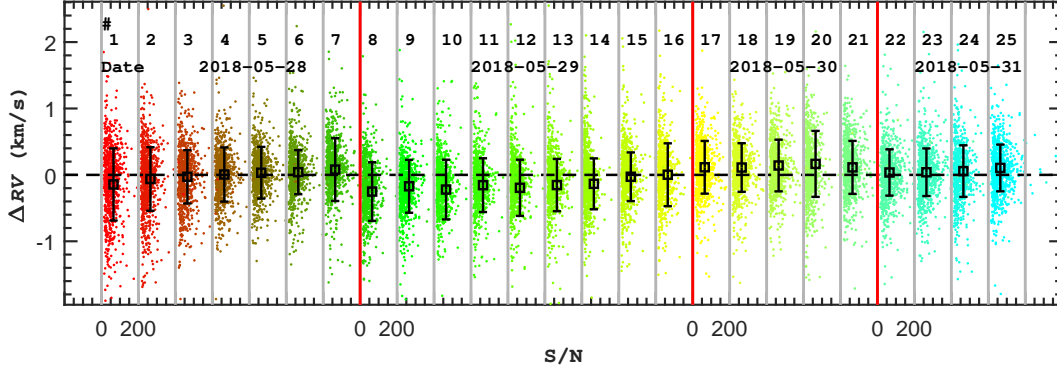


Fig. 5: Similar to Figure 4 but according to the times of exposure. The vertical (red) lines indicate the exposure sequences in different nights marked by their dates (UTC) just below the exposure number.

### 3.4 Correction of systematic errors

As shown in the previous section, systematic errors exist among the  $RV$  measurements when they are obtained at different observational times (major factor) and from different spectrographs (minor factor). These errors induce an enlargement of the uncertainties of  $RV$  measurements from the LAMOST medium resolution spectra. In this section, we introduce a technique to handle these systematic errors, which will significantly improve the  $RV$  precision.

We still use the common constant stars to correct the systematic errors. This time, all these stars are divided into  $25 \times 16$  groups by their plate ID and spectrograph ID. We calculate the averaged weights  $\overline{\Delta RV}_{ij}$  with the formula as

$$\overline{\Delta RV}_{ij} = \frac{\sum_k x_k \cdot \Delta RV_{ijk}}{\sum_k x_k}, \quad (1)$$

where the  $x_k$  is the square of  $S/N$ , the index  $k$  denotes the sequence of each star within one group which is identified by its indices  $i \in [1, 25]$  and  $j \in [1, 16]$ .  $\overline{\Delta RV}_{ij}$  are the systematic errors since the  $RV$ s of the common constant stars are independent on its observational time and spectrograph. We can easily correct the systematic errors by applying the formula

$$RV_{corr} = RV - \overline{\Delta RV}_{ij}, \quad (2)$$

where the  $RV$  (with the omission of the subscript  $i, j, k$ ) is the measured radial velocity from the LAMOST pipelines.

Figure 6 shows the distribution of the  $\Delta RV$ s before and after correcting the systematic errors. The distribution of  $\Delta RV$ s now is unimodal centering around zero with a slight shift of about 0.03 km/s to its uncorrected values, which suggests that the systematic errors have been corrected. The fitting curve shows that the precision of the  $RV$  measurement is a function of the quality of the spectra ( $S/N$ ). We note that the fitting is performed on the data with  $S/N \in [10, 150]$  since the number of spectra with a higher  $S/N$  value is very small and the outlier data points will greatly affect the fitting of the curve. The  $1\sigma$  precision reaches  $\sim 1.3$ ,  $\sim 1.0$ ,  $\sim 0.5$  and  $\sim 0.3$  km/s at  $S/N = 10, 20, 50$ , and  $100$  after the correction, instead of  $\sim 2.9$ ,  $\sim 1.5$ ,  $\sim 0.6$  and  $\sim 0.3$  km/s before the correction, respectively. This correction indicates that the precision

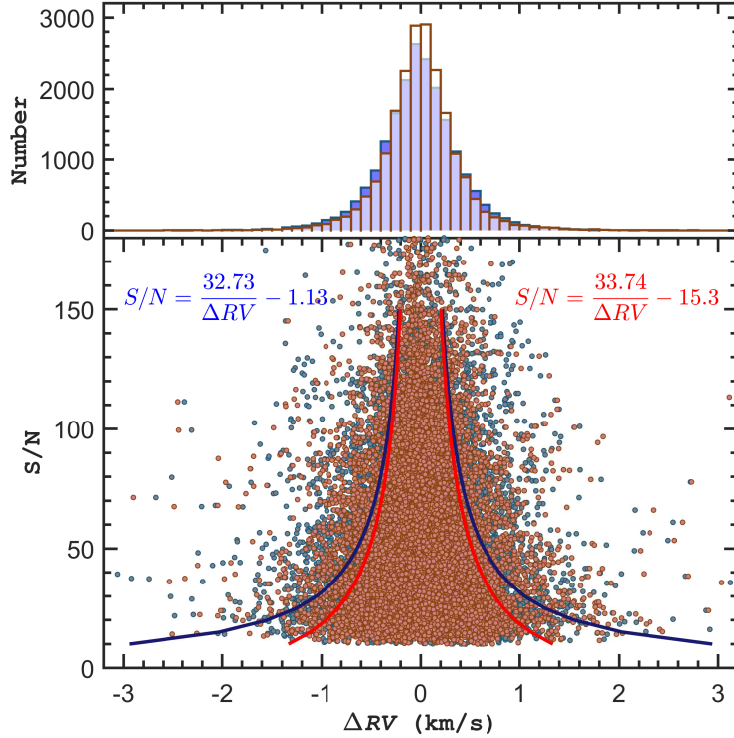


Fig. 6: Similar to Figure 3 but for the constant stars before (in blue) and after (in brown) correction of the systematic errors. The solid curves represent the optimal fitting whose function is given in the bottom panel (see text for details).

## 4 CALIBRATION OF RVs

### 4.1 External errors with APOGEE

As we discussed the internal errors in the above section, in this section, we will discuss the comparison between LAMOST *RV* common constant stars and APOGEE *RV* standard stars. We have cross-identified 34 stars with *RV* measurements in our target list and from Huang et al. (2018), in a range from about  $-110$  km/s to  $50$  km/s. We considered the *RV* values after correction with equation (1). Figure 7 shows the statistical comparison for these 34 stars, where a good agreement between the two data sets can be clearly seen. The optimal fitting is nearly a parallel line to the bisectrix with a zero-point shift of about  $7$  km/s.

### 4.2 An scientific example of combination with photometry

After we determined the external and internal errors, the *RVs* derived from medium-resolution spectra can be calibrated with enough precision. We here merely present one example of science cases where an eclipsing binary star with legacy data from *Kepler* were observed by LAMOST. In this case, the mass of the binary components can be precisely determined (see, e.g., Zhang et al. 2017). KIC 6863229 is such a kind of stars, with  $\alpha(2000) = 19 : 31 : 02.82$ , and  $\delta(2000) = 42 : 19 : 43.10$ , and  $Kp = 12.134^4$ . This star has 25 *RV* measurements from the LAMOST medium-resolution spectra provided here. The light curves are collected from 2009 May 02 to 2013 May 11. Figure 8 shows the two different phase diagrams. Both of the

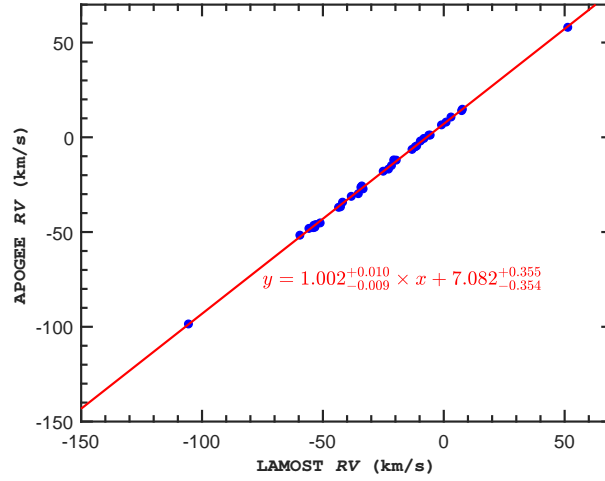


Fig. 7: Statistical comparison of radial velocity between LAMOST and APOGEE. The best linear fit corresponds a line that is nearly parallel to the bisectrix. Note that the error is smaller than the symbol itself.

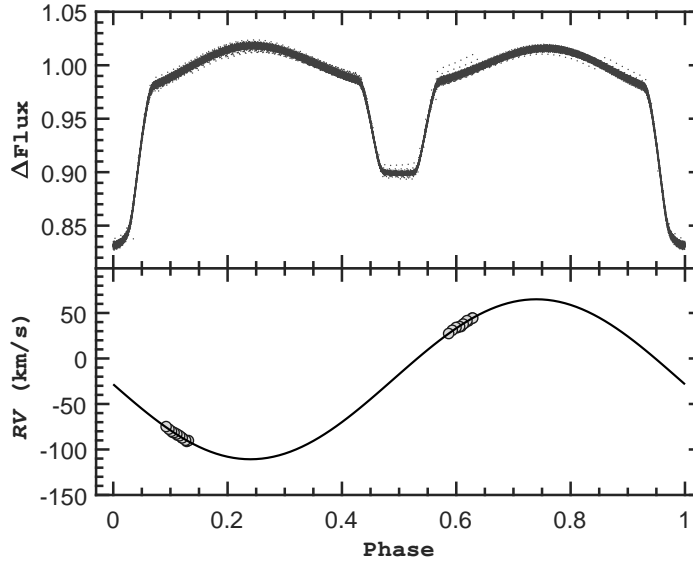


Fig. 8: The fold light curves (top panel) and RVs (bottom panel) of KIC 6863229 as a function of phase. The fitting curve in the bottom panel shows a sinusoidal wave (solid line).

two curves are calculated with the following ephemeris formula

$$\text{Min. } I = \text{BJD } 2454954.485(52) + 1^{\text{d}}.99492(28) \times E, \quad (3)$$

where  $T_0 = \text{BJD } 2454954.485(52)$  and  $P = 1.99492^{\text{d}}$  are the time of a primary eclipse and the available period, respectively, while  $E$  refers to the cycle number. A more detailed analysis of those data can be found in a forthcoming paper (Liu, et al. 2019).

## 5 DISCUSSION

The precision of RVs from LAMOST medium-resolution spectra suffers from slightly and significantly systematic errors induced by different spectrographs and observation times, respectively, particularly for the

observation campaigns with large gaps. The most significant systematic errors are found between different observational nights, which may have zero-point differences of about 0.5 km/s. There also exists a slight drift for the  $RV$  measurements during the same night, typically with a value of a few hundreds m/s. The instrumental effects can account for that, such as the cooling device which is put on the CCDs of LAMOST. Due to fuel consuming, the weight of that device will change and influence the position of spectra where their position is used for calibrating the wavelength. To avoid this, a semi-conductive devices will be used for cooling down the CCDs without changing their weight. The slight systematic errors between different spectrographs are very possibly caused by zero-point differences between these spectrographs, thus, again, changing the wavelengths which are used for deriving  $RV$ s.

Although the  $RV$ s suffer from systematic errors, these errors can be corrected through different techniques. In this paper, we address one method to correct the measured  $RV$ s and the results look reasonable. Our calculation based on 803 common “constant” stars which have  $RV$ s not changing  $> 1$  km/s over time. The systematic errors caused by instrument effects or observational campaigns should be the same to all the stars. Therefore, one can use these stars to evaluate the intrinsic precision of  $RV$  measurement. Our results also give an estimation of the precision for different quality of medium-resolution spectra as indicated by their  $S/N$  in  $SDSS$ -like  $r$  band. After the correction, the precision reaches  $\sim 1.3$ ,  $\sim 1.0$ ,  $\sim 0.5$  and  $\sim 0.3$  km/s at  $S/N = 10, 20, 50$ , and  $100$ , which the corresponding values before correction are  $\sim 2.9$ ,  $\sim 1.5$ ,  $\sim 0.6$  and  $\sim 0.3$  km/s, respectively. Another technique is to calculate differential  $RV$ s before re-shifting the  $RV$ s’ zero-points, which is very similar to the measurement of differential magnitudes for variable stars in photometry (Pan et al. in Prep.). Our method should also draw one attention to the low-resolution spectra probably suffer from systematic errors as well. However, time series plates are only obtained for a low percentage of plates. The better way to remove systematic errors in low-resolution spectra can be using some standard  $RV$  stars based on a similar technique.

The external errors of LAMOST are also calculated through 34 common stars with APOGEE catalog from Huang et al. (2018). We have found a systematic difference of  $\sim 7$  km/s between those two data sets. We discussed an example of an eclipsing binary star, whose calibrated  $RV$  curve with reasonable accuracy was analyzed in combination with the *Kepler* photometry. This could be very useful to derive robust fundamental parameters for such stars, in particular for masses (Zhang et al. 2017).

## 6 CONCLUSION

A plate in the *Kepler* field had been observed by LAMOST with the medium-resolution spectrographs and produced through the most updated pipelines with  $RV$ s. These multiple visiting targets offer an opportunity to test the accuracy and precision of the  $RV$ s derived from this new system. By analyzing the 25 plates obtained through 2018 May 28 -31, we find that there are systematic errors between different spectrographs and observational campaigns. However, these errors can be well removed by dividing the targets into different groups according to the two observational factors. The internal errors for  $RV$ s are found to be with the values of 1.3, 1.0, 0.5 and 0.3 km/s at  $S/N = 10, 20, 50$ , and  $100$ , respectively. We also compare our results with the APOGEE  $RV$  standard stars and find the external error is about 7 km/s based on 34 common

We end this paper with the remark that the precision of  $RV$ s of medium-resolution spectra is a fundamental measurement for the medium-resolution survey of LAMOST in the next five years, as well as the atmospheric parameters. The scientific goals that can be studied with such spectra are built on these precision.

**Acknowledgements** The Guoshoujing Telescope (the Large Sky Area Multi-object Fiber Spectroscopic Telescope LAMOST) is a National Major Scientific Project built by the Chinese Academy of Sciences (CAS). Funding for the project has been provided by the National Development and Reform Commission. LAMOST is operated and managed by the National Astronomical Observatories, CAS. We acknowledge the helpful discussion with Peter De Cat that improves the manuscript. JNF acknowledges the support from the National Natural Science Foundation of China (NSFC) through the grant 11673003 and 11833002. WKZ acknowledges the support from the China Postdoctoral Science Foundation through the grant 2018M641244 and the LAMOST fellowship as a Youth Researcher which is supported by the Special Funding for Advanced Users, budgeted and administrated by the Center for Astronomical Mega-Science, Chinese Academy of Sciences (CAMS). XQC and YHH are supported by Key Research Program of Frontier Sciences, CAS, through the grant QYZDY-SSW-SLH007.

## References

- Adelman-McCarthy, J. K., Agüeros, M. A., Allam, S. S., et al. 2006, *ApJS*, 162, 38
- Alam, S., Albareti, F. D., Allende Prieto, C., et al. 2015, *ApJS*, 219, 12
- Binney, J., & Merrifield, M. 1998, *Galactic astronomy* / James Binney and Michael Merrifield. Princeton, NJ : Princeton University Press, 1998. (Princeton series in astrophysics) QB857 .B522 1998 ,
- Borucki, W. J., Koch, D., Basri, G., et al. 2010, *Science*, 327, 977
- Cui, X.-Q., Zhao, Y.-H., Chu, Y.-Q., et al. 2012, *Research in Astronomy and Astrophysics*, 12, 1197
- De Cat, P., Fu, J. N., Ren, A. B., et al. 2015, *ApJS*, 220, 19
- Eisenstein, D. J., Weinberg, D. H., Agol, E., et al. 2011, *AJ*, 142, 72
- Gaia Collaboration, Brown, A. G. A., Vallenari, A., et al. 2018, *A&A*, 616, A1
- Ge, J., Mahadevan, S., Lee, B., et al. 2008, *Extreme Solar Systems*, 398, 449
- Gilliland, R. L., Brown, T. M., Christensen-Dalsgaard, J., et al. 2010, *PASP*, 122, 131
- Gunn, J. E., & Griffin, R. F. 1979, *AJ*, 84, 752
- Huang, Y., Liu, X.-W., Chen, B.-Q., et al. 2018, *AJ*, 156, 90
- Luo, A.-L., Zhang, H.-T., Zhao, Y.-H., et al. 2012, *Research in Astronomy and Astrophysics*, 12, 1243
- Luo, A.-L., Zhao, Y.-H., Zhao, G., et al. 2015, *Research in Astronomy and Astrophysics*, 15, 1095
- Marconi, M., Molinaro, R., Bono, G., et al. 2013, *ApJ*, 768, L6
- Nidever, D. L., Marcy, G. W., Butler, R. P., Fischer, D. A., & Vogt, S. S. 2002, *ApJS*, 141, 503
- Pinsonneault, M. H., Elsworth, Y., Epstein, C., et al. 2014, *ApJS*, 215, 19
- Pinsonneault, M. H., Elsworth, Y. P., Tayar, J., et al. 2018, *ApJS*, 239, 32
- Prša, A., Batalha, N., Slawson, R. W., et al. 2011, *AJ*, 141, 83
- Stoughton, C., Lupton, R. H., Bernardi, M., et al. 2002, *AJ*, 123, 485

- Wang, S.-G., Su, D.-Q., Chu, Y.-Q., Cui, X., & Wang, Y.-N. 1996, *Appl. Opt.*, 35, 5155
- Xing, X., Zhai, C., Du, H., et al. 1998, *Proc. SPIE*, 3352, 839
- Zhang, X. B., Fu, J. N., Liu, N., Luo, C. Q., & Ren, A. B. 2017, *ApJ*, 850, 125
- Zhao, G., Zhao, Y.-H., Chu, Y.-Q., Jing, Y.-P., & Deng, L.-C. 2012, *Research in Astronomy and Astrophysics*, 12, 723
- Zong, W., Charpinet, S., Vauclair, G., Giammichele, N., & Van Grootel, V. 2016, *A&A*, 585, A22
- Zong, W., Fu, J.-N., De Cat, P., et al. 2018, *ApJS*, 238, 30